Geophys. J. Int. (2007) **168,** 983–998 doi: 10.1111/j.1365-246X.2006.03278.x

Geophysical characteristics of the ultraslow spreading Gakkel Ridge, Arctic Ocean

Wilfried Jokat and Mechita C. Schmidt-Aursch

Alfred Wegener Institute for Polar and Marine Research, Columbusstrasse, D-27568 *Bremerhaven, Germany. E-mail: jokat@awi-bremerhaven.de*

Accepted 2006 November 3. Received 2006 October 31; in original form 2005 August 31

SUMMARY

The northernmost spreading centre of the world, the Gakkel Ridge, is also an end-member in terms of global spreading velocities. Models show that full spreading rates vary between 1.3 and 0.63 mm yr^{-1} along the almost 1800 km long ridge system in the Central Arctic Ocean. The western part of the ridge was investigated in great detail by a two-ship expedition in summer 2001. The complete data sets and the modelling of the seismic refraction and aeromagnetic experiments gathered during this expedition are shown in this study. The magnetic signals along the dense (2 km spacing) aeromagnetic flight lines acquired at the same time show a good correlation between high amplitudes and a shallowing of the rift valley and the presence of large volcanic constructions at the rift shoulders. The magnetic anomalies rapidly fade out east and west of these centres of focused magmatism. This might indicate that the basaltic layer producing the magnetic anomaly thins away from the volcanic centres. A continuous magnetic anomaly is observed along the rift valley west of 3°30′E, consistent with increasing and more robust magmatism.

The crustal thickness along the Gakkel Ridge varies greatly. Beneath some of the centres of focused magmatism, the oceanic crust thickens up to 3.5 km. In the amagmatic segments in between the crust thins to 1.4–2.9 km. This observation is also valid for the Western Volcanic Zone west of 3°30′E, where despite the stronger magnetic anomaly the crust does not significantly thicken. The strength of the magnetic anomaly along the rift valley is thus not a reliable indicator of crustal thickness beneath the Gakkel Ridge. The data show that the crustal thickness does not change dramatically across 3°30′E. Only the occurrence of a large elongate volcanic ridge significantly influences this parameter. More frequent volcanic eruptions along such ridges are most likely responsible for the basalts found in the westernmost part of the Gakkel Ridge. In the non-transform segments some seismic stations indicate that mantle rocks are exposed at the seafloor, with no indication of the presence of a basaltic cover or normal oceanic crust. Both the seismic and magnetic data support models in which the uppermost basaltic cover is responsible for the magnetic anomaly in the rift valley.

Key words: Arctic Ocean, crustal thickness, Gakkel Ridge, ultraslow spreading.

INTRODUCTION

At the beginning of geoscientific research in the Arctic ocean, even bathymetry was poorly known and the existence of an active mid-ocean ridge in the central Arctic was quite speculatively based on sparse earthquakes lining up systematically in the middle of the Eurasia Basin. In the 1970s, aeromagnetic investigations were the only geophysical experiments that were not hindered by the pack ice. Karasik (1968) and Vogt *et al.* (1979) reported on regional aeromagnetic surveys across the Arctic Ocean, which provided the first detailed insight into the tectonic evolution of the Eurasia Basin. According to their still valid geodynamic model, the Eurasia Basin began to form in the early Cenozoic at approximately 55 Ma. As a consequence, a continental fragment, the Lomonosov Ridge, rifted away from the Barents and Siberian shelves. The part of the ridge west of 3°30′E formed only for some 35 Ma, when a propagation of the rift split the Morris Jessup Rise from the Yermak Plateau. Since then the Lena Trough developed in the centre of the Fram Strait. Today the Gakkel Ridge is known to be located in the centre of the Eurasia Basin, and is connected to the global mid-ocean ridge system via the Lena Trough and the Molloy/Knipovich ridges. The Gakkel Ridge is anomalously deep and is the slowest spreading ridge in the global ridge system. During most of its evolution, full spreading rates were below 1.5 cm yr^{-1}. Global studies of plate movements (NUVEL-1A, DeMets *et al.* 1994) suggest that the recent spreading rates at the western part of the ridge, north of Svalbard, have a full

rate of 1.3 cm yr^{-1}, decreasing to 0.6 cm yr^{-1} at the termination of the ridge close to the Laptev Sea. Geophysical investigations from drifting ice islands west of 20°E provided the first information on the crustal structure of the ridge and the adjacent basins. The thickness of the oceanic crust varies between 2 and 3 km in the investigated areas (Duckworth *et al.* 1982; Jackson *et al.* 1982). The only seismic data on crustal thickness from the Gakkel Ridge were acquired during the FRAM expeditions close to 0° in the late 1970s (Kristoffersen *et al.* 1982). Here, a crustal thickness of 6–7 km was reported for the oceanic crust at the Gakkel Ridge.

These older experiments provided no consistent view of the thickness of the oceanic crust. From the sparse data set, two important observations were made: (1) the thicker crust was associated with high magnetic amplitudes, while areas with a reduced field seemed to correlate with thinner oceanic crust, and (2) high magnetic amplitudes in the rift valley seemed to correlate with a shallowing of water depth.

Based on seismic observations in the Arctic, Reid & Jackson (1981) introduced a model for oceanic crust formation that predicts a significant decrease in crustal thickness for full spreading rates less than 15–20 mm yr^{-1}. However, this model was quite disputed since the database at that time was very sparse and similar observations from other areas were not available. Seismic investigations along other slow spreading ridges, like the Mohns (Klingelhöfer *et al.* 2000), Knipovich (Crane *et al.* 2001; Ljones *et al.* 2004; Ritzmann *et al.* 2004), and Southwest Indian (Muller *et al.* 1999) ridges, in the last decade, however, have confirmed the existence of thin crust (∼3–4 km) below their rift valleys. Theoretical models, which predict conductive cooling and upwelling processes to explain the observations came to be widely accepted (Reid & Jackson 1981; Bown & White 1994). These seismic studies showed also that the velocity structure at slow spreading ridges differs significantly from that of normal oceanic crust. Seismic velocities above 6.5 km s^{-1} are rarely observed indicating that oceanic layer 3 is missing, or very thin beneath such ridges.

Before the most recent expedition to the Gakkel Ridge in 2001, only gravity and bathymetric studies were published on the crustal structure of ridge (Coakley & Cochran 1998; Weigelt & Jokat 2001; Cochran *et al.* 2003). The first two studies indicate that thin crust with a thickness of 2–4 km may be present beneath the rift valley and off-axis, which was regarded to be normal for oceanic crust formed at ultraslow spreading mid-ocean ridges. Since no seismic refraction data were available to constrain the gravity model, the reported crustal thicknesses of 2–4 km for the rift valley were not uniquely constrained. The thin crust, however, contradicted the findings of Kristoffersen *et al.* (1982).

Almost 20 yr after the first geophysical investigations of the Gakkel Ridge, a geoscientific expedition in the summer 2001 with the research icebreakers RV Polarstern and USCGC Healy investigated almost 2/3 of the topographically well-exposed western Gakkel Ridge. The programme included both geophysical (Jokat *et al.* 2003) and petrological experiments (Michael *et al.* 2003). As a result, more than 200 locations were successfully dredged (Fig. 1), and an almost complete swath bathymetry is now available for the investigated ridge segment. Seismic and magnetic investigations were carried out to clarify the significance of the early geophysical observations and results. All the data sets showed that global models for mid-ocean ridge structure do not predict the features observed at Gakkel Ridge (Michael *et al.* 2003; Jokat *et al.* 2003). The ridge is much more magmatic than previously thought, and hydrothermal activity seems to be much higher than along other mid-ocean ridges (Edmonds *et al.* 2003). Geophysical investigations showed that thin oceanic crust, with a thickness of 1.4–3.5 km, is present. Crustal thickness shows no direct correlation with spreading rates (Jokat *et al.* 2003). This work also showed that the velocity structure beneath some of the volcanic centres is different from the velocity structure between them, though such differences were not identified east of 3°30′E. Finally, this led to the introduction of a new class of mid-ocean ridges, the ultraslow ridges namely the Gakkel and Southwest Indian ridges (Dick *et al.* 2003).

Jokat *et al.* (2003) published a subset of the geophysical data gathered during the expedition. Between 15°E and 55°E, five seismic 1-D depth models and the magnetic line data in this area were shown. No data from the westernmost part of the ridge were shown. In this contribution, the complete new seismic data set, especially for the western part of the Gakkel Ridge, and the complete magnetic data set will be shown as well as their final modelling.

EXPERIMENTAL SET-UP AND MODELLING TECHNIQUES

Seismic refraction

Conducting deep seismic sounding experiments in the pack ice of the Arctic Ocean is an exercise that is completely different from conventional investigations. Pack ice does not allow for the deployment of conventional ocean bottom seismometers, since their safe recovery is almost impossible. The same is true for towing wide airgun arrays and/or a number of large volume airguns. For such experiments two research ice breakers are needed, one lead vessel to break the ice, and a second one with the towed equipment. The gear is towed in a narrow channel of ice-free water behind the ship (Jokat *et al.* 1995).

Consequently, we deployed seismic recording systems on the pack ice. Since we could only use an airgun array with a total volume of 24 l, efforts were made to make the receiver side more sensitive. Instead of a single geophone, an array of geophones was deployed recording the vertical component only. We did not try to design a layout of the geophone array to allow some directional sensitivity, since the geophones drifted with the ice floe during the measurements (Fig. 2). The preferred setup for the seismic stations consists of two separate channels each connected with 8 geophone-chains. For each chain, a 0.4 × 6 m shaft was dug through the snow and firn cover, to reach the more compact ice body (Jokat *et al.* 2002). Care was taken to avoid deployment into melted portions of floes, where small differences of rigidity of the ice body might cause the geophone to tilt into the ground. After deployment of the geophones, the shafts were covered with snow.

Only at some of the first stations was an additional hydrophone deployed, at minimum water depths of around 20 m. Later on, most stations were deployed in the centre of a floe, and we made no attempts to drill through the floe in order to deploy more hydrophones. Data from the hydrophones, in general, were of poorer quality than those from the geophones.

In total, seismic refraction data were acquired at 18 different locations and profiles, whenever possible with stations at the start and end of the profile (Fig. 1). Having two stations out on ice floes often created problems with the geometry since the ships were not able, in some cases, to approach within 5 km the station due to unfavourable ice conditions. Furthermore, the profiles are not straight due to the necessity of steaming around large floes.

The profile lengths varied between 30 and 50 km. The signal to noise ratio on most of the records is close to 1, or even below.

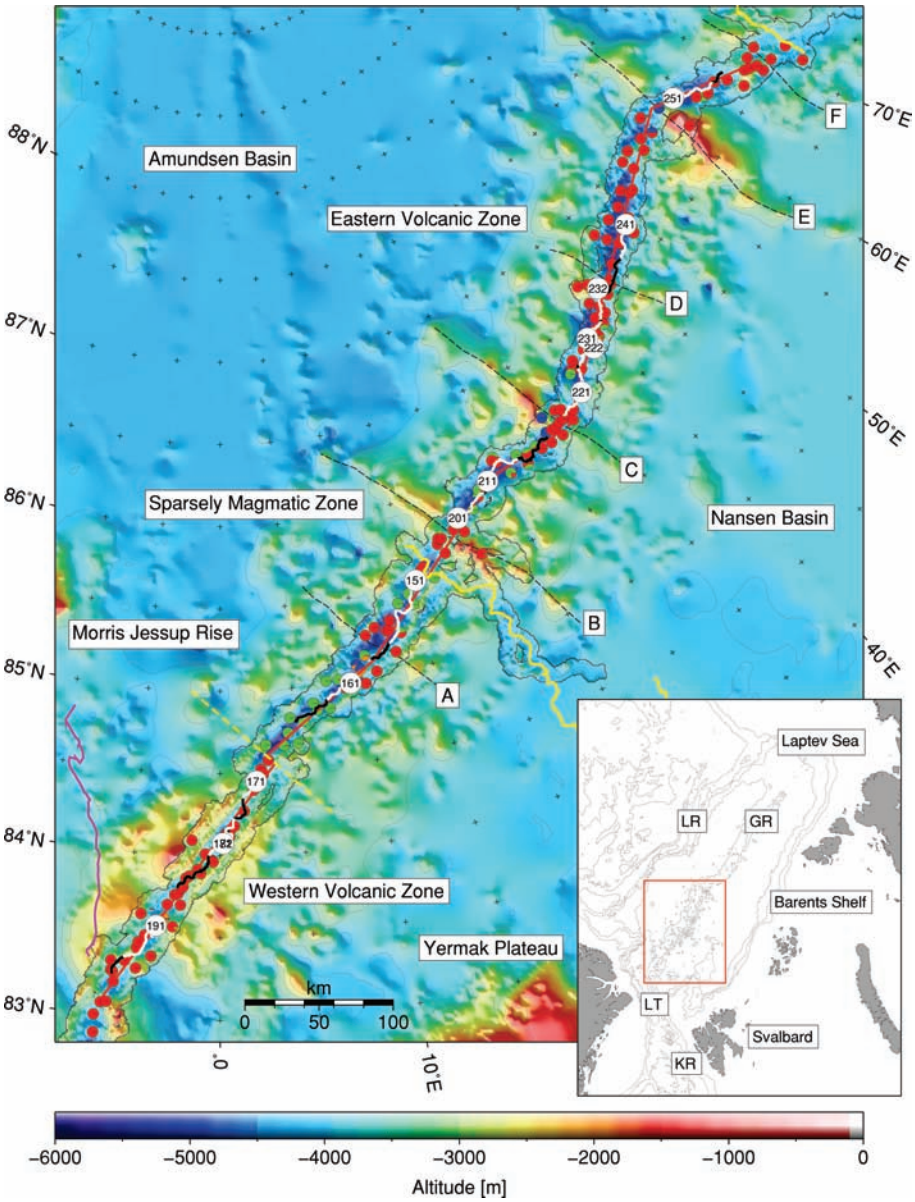

Figure 1. Overview of the Gakkel Ridge investigated during the AMORE 2001 expedition. The bathymetry is a combined grid of ICBAO (Jakobsson *et al.* 2001) and new data collected during the cruise. The white circles indicate the locations and station numbers of the seismic recording stations. The thin white/black lines away from the circles mark the seismic refraction profiles. The white part of the profile indicates the offset range where seismic signals could be identified. Coloured circles show the rock type as percentage of the dredge content (red: Basalt; green: Peridotite, orange: Gabbro, blue: others). The large basement ridges are marked with black dashed lines and named A–F. The yellow lines show the locations of the seismic reflection profiles in the adjacent basins. The pink line marks the drift path of FRAM I. The yellow dashed line marks the boundary between the Western Volcanic Zone and the Sparsely Magmatic Zone at 03°30′E. Inset: IBCAO bathymetry north of Greenland and Svalbard with 1000 m contours, LR: Lomonosov Ridge, GR: Gakkel Ridge, LT: Lena Trough, KR: Kolbeinsey Ridge.

However, the shooting interval (mostly 30 s; shot point spacing 80 m) provided enough coherent energy to allow a safe identification of the traveltime branches in the record sections. Most of the unreversed record sections clearly show traveltime branches with crustal velocities less than 6.5 and more than 7.6 km s^{-1} for the mantle refractions. Fast arrivals from the mantle occur between 6 and 12 km offset from the station and can be followed, in one case, for up to 50 km (Station 151).

For estimating the errors of our models we first discuss the drift of the instruments. If the distance between the shots and a drifting receiver is calculated with a fixed receiver position, the offset is generally wrong, due to the ice drift. Typical drift paths of two stations, 151 and 152, are shown in Fig. 2. The error in determined velocity, assuming a profile length of 60 km and a linear drift of 2.5 km parallel to the profile, for rms-velocities of 1.50 and 5.00 km s^{-1} is as follows:

rms − Vel.	Error
1.50 km s^{-1}	± 0.05 − 0.06 km s^{-1}
5.00 km s^{-1}	± 0.2 − 0.21 km s^{-1}

To eliminate these errors, true receiver positions were calculated by linear interpolation between the hourly GPS-receiver-positions.

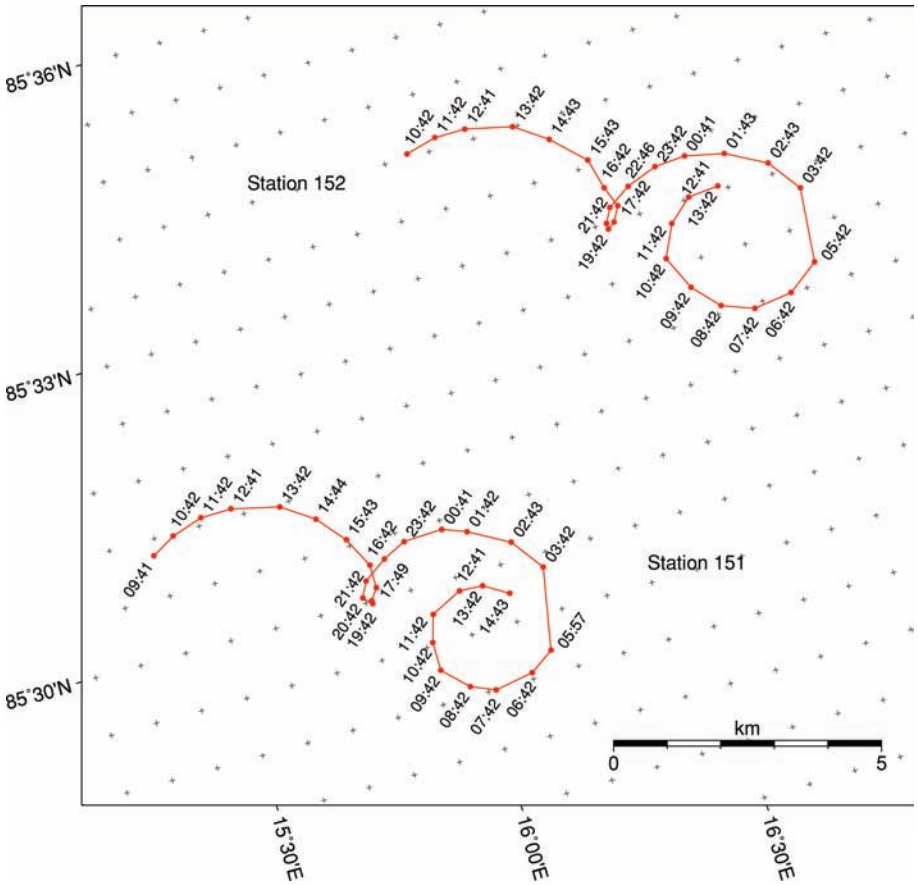

Figure 2. Drift paths of stations 151 and 152 at around 16°E. The stations were placed on the floes for 29 hr (151) and 27 hr (152), respectively.

The RefTek data acquisition unit is equipped with a GPS-antenna to synchronize the internal clock to UTC-time. The GPS-position is recorded every hour. Thus, a picking error of 50–100 ms was chosen for all sections.

To estimate the error for the seismic velocities we have to consider two scenarios:

(i) Some stations do not show any upper crustal phase at all, but only refracted arrivals from the upper mantle. Thus, an error estimate for crustal velocities is not possible. According to information from other stations in such cases we have chosen low seismic velocities ($\sim$3.0 km s^{-1}) at the seafloor and a smooth velocity gradient for deeper levels to fit the traveltime and onset of the upper mantle phase.

(ii) For stations with clear upper crustal phases, we varied the velocities in each layer independently as long as the fit to the traveltime curve was acceptable within the error bars. A second criterion was that the modelled traveltimes should fit, in general, the slope of the traveltime branch. The error for the velocities varied by $\pm$0.2–0.3 km s^{-1}.

Finally, it should be noted that almost all profiles were unreversed. Thus, the calculated seismic velocities are apparent velocities, which might change, if the dips and/or lateral variations of the seismic velocities within the oceanic crust were to become known.

Finite Difference modelling

The kinematic ray tracing technique uses a high-frequency approximation of the wave equation, which leads to the description and representation of propagating waves as rays. In contrast, the finite difference method (FD) calculates the complete wavefield. This allows much more detailed studies of the generation and propagation of refracted and reflected phases. To approximate the wave equations numerical, differential operators replace partial derivatives. Space and time are sampled on a rectangular grid and equal-spaced time steps, respectively. Our modelling uses the program FDVEPS (Bohlen 2002), which computes wavefields in inhomogeneous viscoelastic media. For our purposes, a fully elastic medium is sufficient however, so only the density and seismic *P*- and *S*-wave velocities are required. The FD grid was built up of 3001 $\times$ 1501 cells with 10 m spacing and was calculated with time steps of 0.5 ms. The ray-tracing modelling provided seismic *P*-wave velocities. Furthermore, a constant Poisson's ratio of 0.25 was assumed to calculate *S*-wave velocities. Densities between 2.6 and 2.8 $\times$ 10^{-3} kg m^{-3} were assigned to the oceanic crust, and the upper mantle was modelled with a constant density of 3.3 $\times$ 10^{-3} kg m^{-3}. A Ricker-wavelet with a centre frequency of 7 Hz was chosen for the source signal. In this study the approach was used in order to have an independent numeric control on the existence of PmP reflections from the crust–mantle boundary, which is not obvious from the record sections. Furthermore, the method allowed us to better interpret some arrivals, for example, *P*–*S* conversions.

The thin/hidden layer problem

One characteristic of the traveltime curves from most of the record sections is the absence of a clear PmP phase marking the

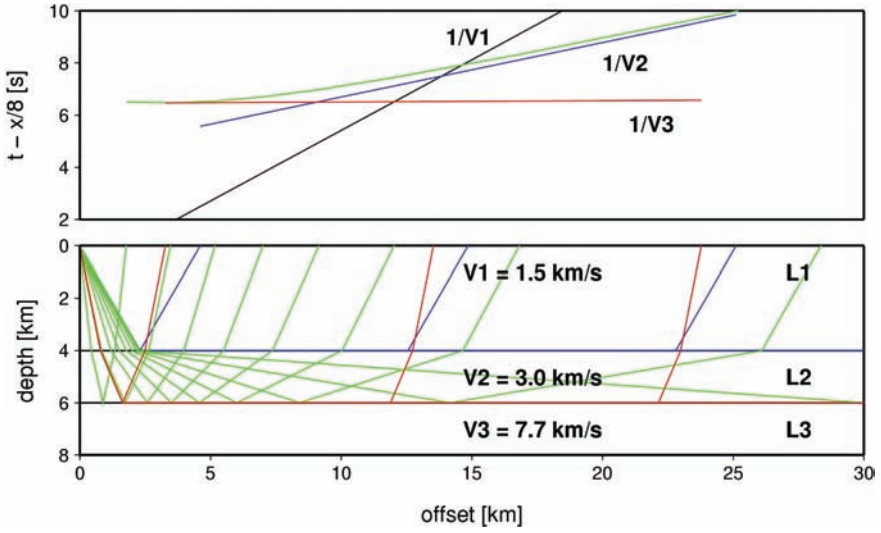

Figure 3. Simplified model with constant layer velocities to explain the problem identifying crustal phases at some recording stations.

crust–mantle transition. This may lead to the conclusion that no sharp transition zone between crust and mantle exists, but instead a thick velocity gradient zone. The FD modelling independently proves that this view is wrong. The PmP phase is present, but not visible in the data, as it is hidden within the strong wave trains of the water waves and some chaotic reflections. Some indications for the presence of the PmP can be seen in the near offsets although the signals are very weak. Other hints occur in the form of strong amplitudes in offset ranges, where the reflected and refracted arrivals constructively interfere. To better display this specific problem, we have added a FD synthetic panel.

Another scenario for a hidden layer is a seismic layer, whose thickness is small compared to the overburden layer (Fig. 3). In our case, this would be a thin oceanic crust overlain by a much thicker water column. Head waves are produced in the oceanic crust and in the upper mantle. However, since the oceanic crust is thin also compared to the water depth, and the seismic velocity of the upper mantle is larger than in the crust, the head wave from the crust is overtaken by the rapidly travelling head wave coming from the upper mantle before it can overtake the direct arrival. In our data, arrivals from the oceanic crust are observed as second arrivals, which can only be present if no strong velocity gradient like that in normal oceanic crust (layer 2–layer 3) exists.

Modelling criteria

A characteristic feature of most record sections presented in this study is the missing information on the seismic velocities for the uppermost layer. This is a direct consequence of the experimental set up with source and receiver at sea level, and the water depths of up to 5000 m. Because of this, seismic velocities as low as 2.4 km s^{-1} have been assumed for the uppermost layer. Such velocities are reported from various surveys along mid-ocean rift valleys (Grevemeyer & Weigel 1996). The velocity gradient for this uppermost layer has been chosen in such a way that the onsets of the later arrivals are correct. At various stations, seismic velocities of 4.0–5.0 km s^{-1} are observed. Higher velocities, of slightly more than 6.0 km s^{-1}, are only observed at four stations that are close to large volcanic features. On several record sections no crustal phases are observed at all. Again, this might be due to the limited data quality, but most likely to the geometrical hidden layer problem. In these cases a velocity model has been chosen similar to neighbouring stations, where lower crustal traveltime branches are visible. A second criterion for the modelling in such cases was the intercept time of the mantle refraction, which allows a first order comparison of crustal thicknesses between different stations, assuming the velocity structure of the crust is homogeneous. We have chosen a conservative model (slow velocities) for these sections based on the information available, although other models are possible.

In the very deep part of some profiles, the upper mantle reflection might strongly interfere with the lower crustal refractions due to the hidden layer problem. The seismic nature of the crust–mantle transition cannot be resolved in detail with the data presented here. Thus, the crust–mantle boundary has been modelled as a first order boundary. On almost all record sections, the upper mantle refraction, Pn, is observed at varying offsets with velocities varying between 7.4 and 7.8 km s^{-1}. Although stations were deployed at both ends of several profiles, the distance between the recording sites was too large to provide a reversed line.

Aeromagnetic investigations

In the past decades, Russian and US institutions have carried out extensive aeromagnetic surveys with line spacing of approximately 20 km to decipher the tectonic history of the Arctic basins. In the Eurasia Basin first order observations showed that magnetic anomalies are highly variable along the rift valley of Gakkel Ridge (Vogt *et al.* 1979; Verhoef *et al.* 1996). Vogt *et al.* (1979) and Jackson *et al.* (1982) noted that high magnetic amplitudes are closely related to a shallower rift valley. They correlated normal oceanic crust with high magnetic amplitudes, and thin oceanic crust with calm magnetic zones. However, the line spacing and the poorly known bathymetry prevented any convincing explanation of the observations. Thus, the purpose of our magnetic investigations was to densify the existing flight pattern wherever possible across the rift valley. A line spacing of 2 km was chosen as being the best compromise between target depth, available flight time and the expected spatial resolution necessary to distinguish between different tectonic units. Due to the tight flight schedule, it was not possible to deploy a magnetic base station to monitor the diurnal variations of the earth's magnetic field close to the flight area. However, diurnal data from NyÅlesund (Spitsbergen) were used to subtract the long-term variations.

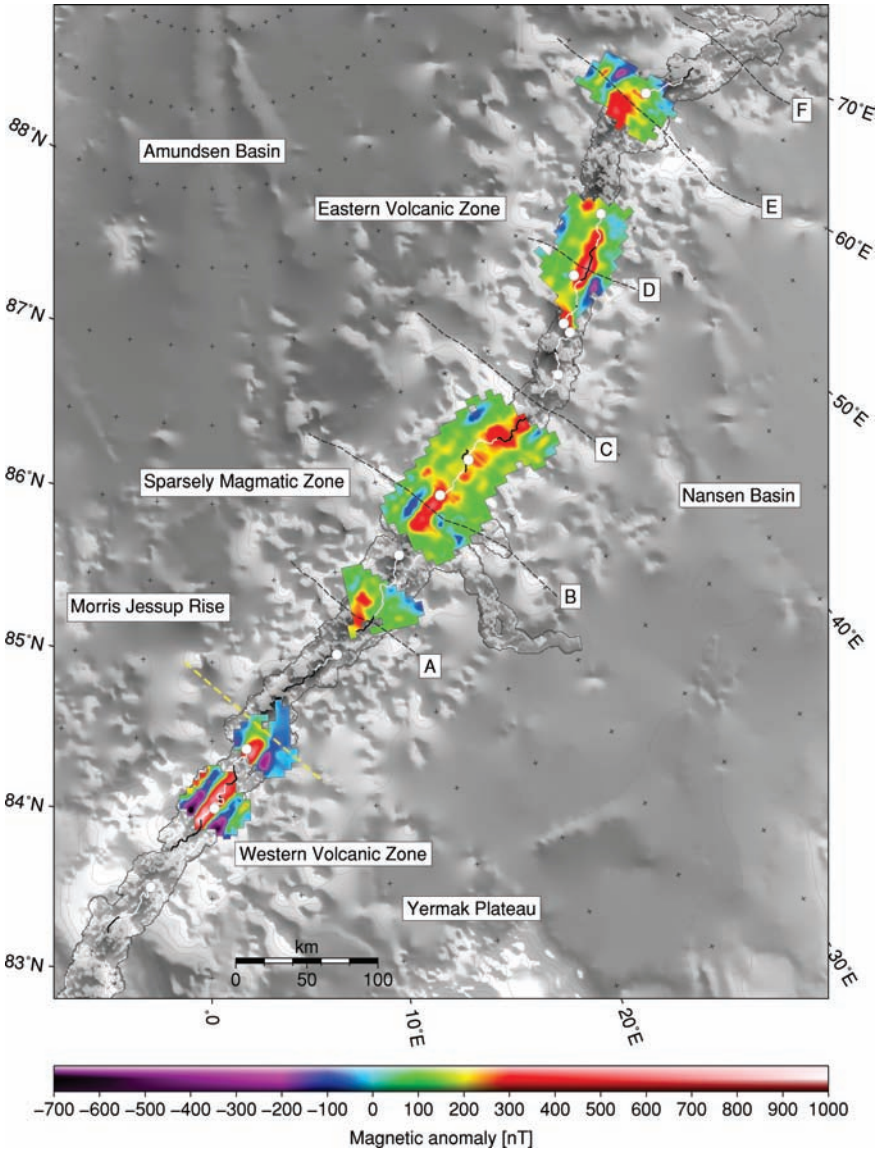

Figure 4. Magnetic data gathered at the different segments of the Gakkel Ridge. The bathymetry is plotted in grey. The seismic stations and basement ridges are displayed. The yellow dashed line indicates the boundary between the WVZ and SMZ at 03°30′E.

Furthermore, the quality of the magnetic data was checked by cross lines. In several instances there are distinct shifts between adjacent lines flown at different times. All data were adjusted not only for diurnal variation but also for different flight levels (Fig. 4). During levelling the first vertical derivative of the data was used as a quality criterion to identify shifts between the lines. The misties were then minimized within the given networks.

In spite of all these problems approximately 56 hr of new magnetic data could be acquired during 14 days of flying (Fig. 3). This corresponds to 8300 km total profile length, assuming a mean flight velocity of 148 km hr^{-1} (Jokat *et al.* 2002). The length of the lines varies between 37 and 56 km.

RESULTS

The description of the wide-angle data is made according to the proposed segmentation of the Gakkel Ridge (Michael *et al.* 2003). Based on bathymetry and the results of the petrological sampling, three major magmato-tectonic provinces were defined along the ridge axis (Fig. 1): the western volcanic zone (WVZ), the Sparsely Magmatic Zone (SMZ), and the Eastern Volcanic Zone (EVZ). They show distinct differences in bathymetry and in potential field data. Please note that the seismic refraction lines were acquired before the swath bathymetry survey was complete and thus, the survey lines could not always be placed in an optimal way. The modelling results are displayed in Figs 5–9, and summarized in Table 1 and Figs 10(a)–(c). Not all seismic sections will be shown in this section. The remaining seismic sections are displayed in Fig. 11.

The Western Volcanic Zone (7°W–3°E)

The magnetic anomaly along the rift valley is continuous and has an amplitude of 500 nT. At the eastern termination of this segment (Fig. 3), the strong positive anomaly diminishes over a distance of 29 km from 300 nT to less than 10 nT. Almost exclusively basalts were dredged in this segment of the Gakkel Ridge (Michael *et al.*

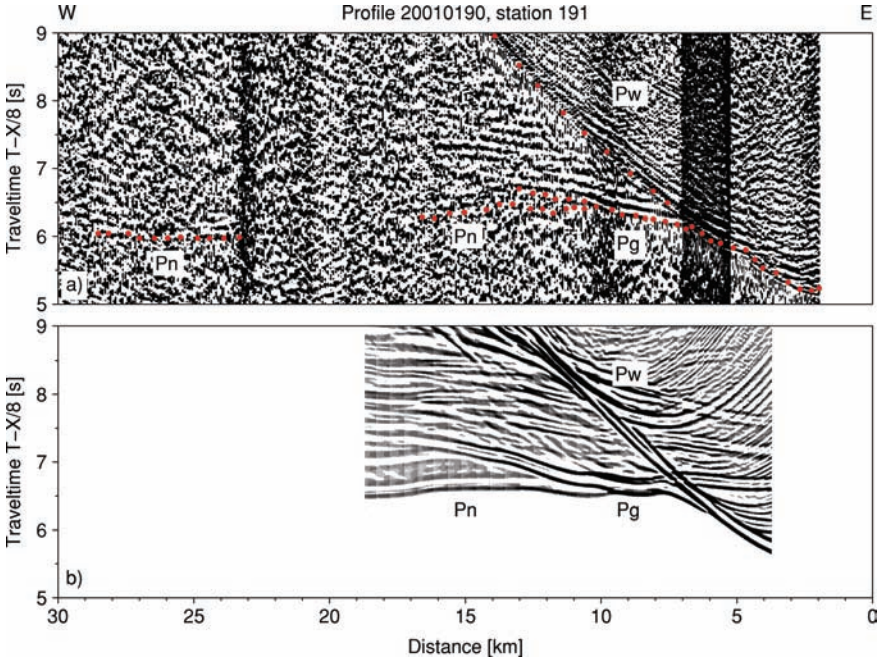

Figure 5. Seismic record section of station 191. Panel information: (a) original data with phase identifications and picks in red, (b) Synthetic data derived by FD modelling. The depth model and the ray coverage are summarized in Fig. 10.

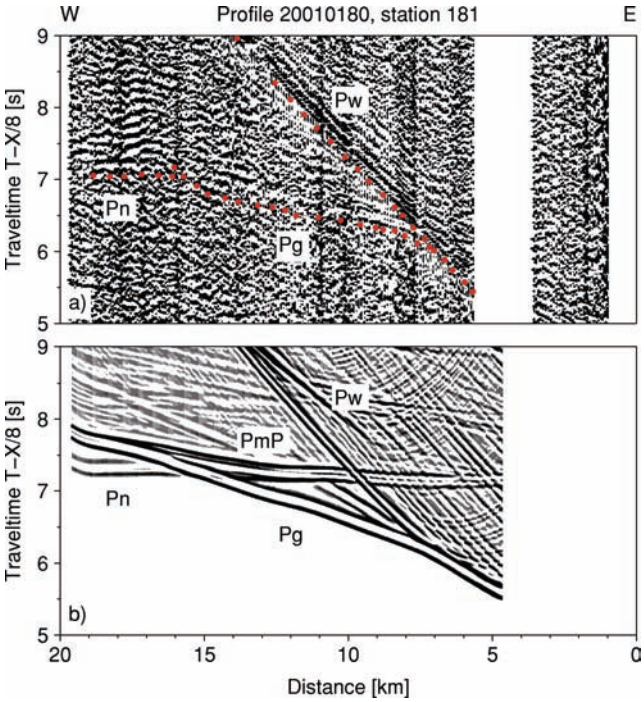

Figure 6. Seismic record section of station 181. For the description of the panels see Fig. 5.

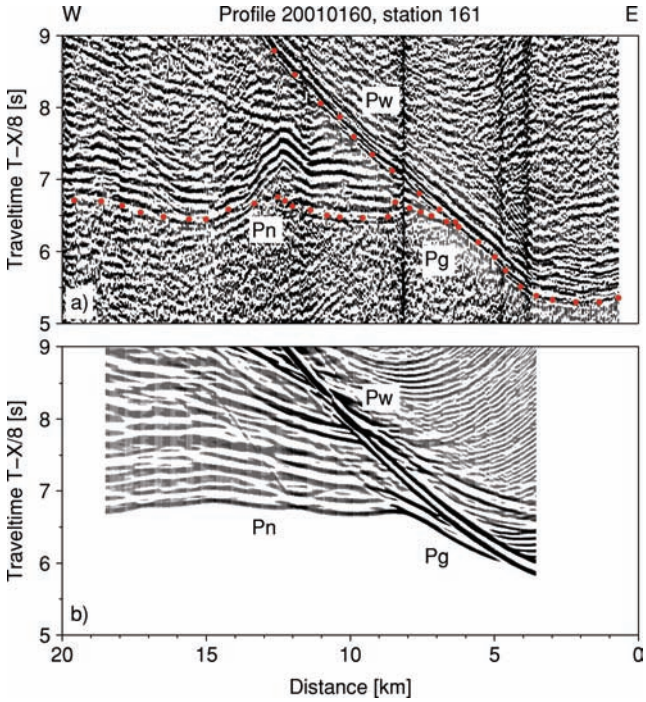

Figure 7. Seismic record section of station 161. For the description of the panels see Fig. 5.

2003). Here, information on the crustal thickness could be acquired along three profiles (20010170, 20010180, 20010190) and at four stations. The positions of the RefTek stations were more driven by weather conditions than by a systematic approach. Large open water areas over the western part of the Gakkel Ridge caused a lot of fog during the acquisition of these lines, which made the deployment or recovery of the stations by helicopter difficult. The description of the results starts in the southwest and proceeds towards the SMZ and EVZ.

Line 20010190 (Figs 5 and 10a)

Station 191 is the westernmost position at which the crust of the Gakkel Ridge was investigated. Only one upper crustal phase, with

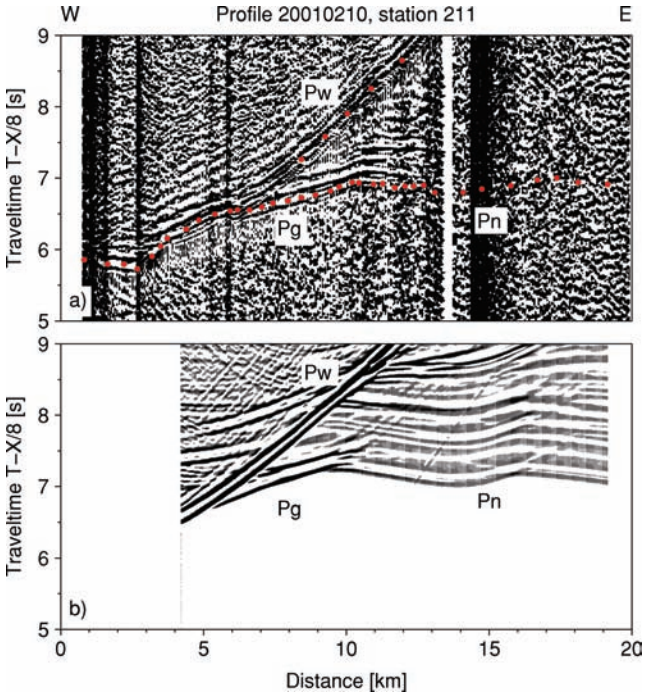

Figure 8. Seismic record section of station 211. For the description of the panels see Fig. 5.

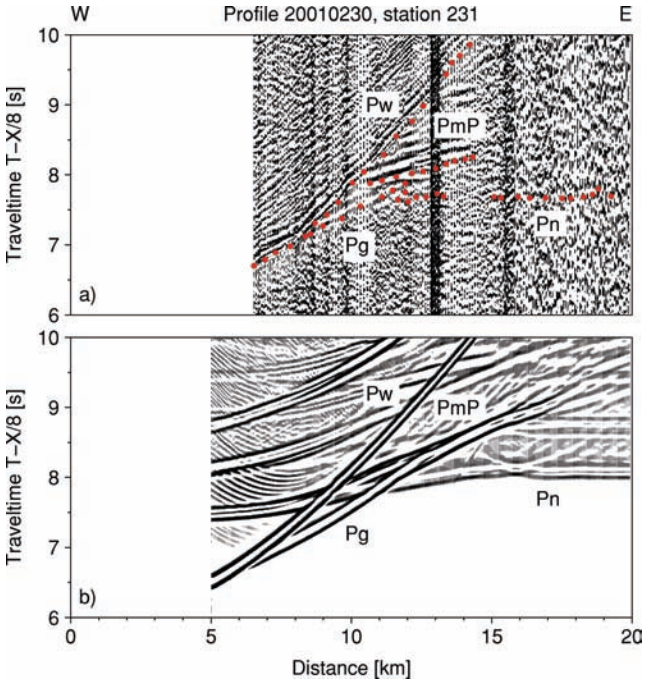

Figure 9. Seismic record section of station 231. For the description of the panels see Fig. 5.

$Vp = 5.0$ km s^{-1}, is visible in the record section at offsets between 7 and 13 km. The onset of the mantle refraction is at approximately 11 km, and has a velocity of 7.7 km s^{-1}. This phase can be traced with confidence to a maximum distance of 17 km. The picked traveltimes at offsets of 23–28 km, however, fit the model although they are less clear in the section. The model starts with a $Vp = 3.0$ km s^{-1} and terminates with a velocity of 5.0 km s^{-1} at the base of the oceanic crust. Velocities above 6.0 km s^{-1} (layer 3) are not observed. The low velocities for the entire oceanic crust are supported by the fact that a slow phase of 4.5–5.0 km s^{-1} is still present as a secondary arrival beyond the crossover distance of the mantle refraction. This indicates that there is no strong velocity gradient in the oceanic crust. The FD modelling confirms the ray tracing model. Furthermore, it shows that both the refracted energy from the upper mantle and the lower oceanic crust came close together and so can hardly be distinguished from one another. No clear PmP can be seen in the FD modelling. The PmP phase is within recording offsets, which are strongly disturbed by the water waves. The crustal thickness varies between 2.2 and 3.5 km.

Line 20010180 (Figs 6 and 10a)

Station 181 is almost located in the middle of the WVZ. A weak upper crustal phase, with a velocity of 4.0 km s^{-1}, can be observed between offsets of 7 and 16 km. A phase with a seismic velocity of 7.6 km s^{-1} appears abruptly at 16 km offset, and is interpreted here as the Pn phase. For modelling, a layer with velocities of 2.4–3.2 km s^{-1} has to be incorporated to make the onset of the 4.0 km s^{-1} phase possible. This layer is 1–1.3 km thick and might represent basaltic rocks, e.g. pillow lavas. A maximum seismic velocity of 5.2 km s^{-1} is introduced to constrain the traveltime branch of the crustal phase at 16 km offset. The mantle refraction can only be followed for a short distance of 3 km. A weak indication for a PmP phase is visible between 12 and 18 km offset. Since it is difficult to pick the first arrival of this phase it has not been included in the ray tracing. At station 181, the crust is 4.9 km thick. No phases supporting the presence of oceanic layer 3 are observed. For station 181, the synthetic seismogram shows a clearly distinguishable phase for the PmP reflection, although no such branch is visible in the data.

The Sparsely Magmatic Zone (3°E–29°E)

The rift valley of this segment is the deepest along the ridge with water depths of up to 5.5 km. It is characterized by the occurrence of large volcanic basement ridges (Fig. 1, A and B). In this 300 km long portion of the ridge less than 20 per cent of the rift valley is covered by basalts (Michael *et al.* 2003). Magnetic amplitude anomalies are low (∼10 nT) along the few lines further to the northeast of ridge A, and increase towards the magmatic basement ridge B, from values around 0 nT to 200–300 nT, and vanish again within a short distance east of it (Fig. 3). The seismic profiles are located between the basement ridges and on top of their bathymetric expression in the rift valley. In total, four seismic refraction lines were acquired at the different structural elements in this segment.

Line 20010160 (Figs 7 and 10b)

The seismic section is dominated by reflections from the water bottom and refraction signals from the crust–mantle boundary. The onset of the mantle refraction is approximately at 8 km offset with a seismic *P*-wave velocity of 7.7 km s^{-1}. The variations of the traveltime curve are mainly due to the ship's course and the water depth. Since the travelled ray path is not identical with the measured water depths, not all undulations of the traveltime curve could be ray traced by 2-D modelling. In this section, only signals with a *P*-wave velocity of about 4.5 km s^{-1} are observed from the crust. It is a short phase at offsets between 6 and 7 km. Thus, the velocity model starts at the seafloor with 4.0 km s^{-1} and reaches 6.0 km s^{-1} at the bottom

Table 1. Summary of the stations along the Gakkel Ridge compared with seismic results from other ultraslow spreading ridges. Stations 152 and 242 were not modelled because of insufficient data quality. Please note that the models for stations 171 and 172 are quite different despite their proximity. This indicates that the crustal composition beneath the stations might be too complex to be imaged by this experimental setup. Layer 2,3: Oceanic layer 2,3; NTS: location is a non-transform segment or in the middle of two basement ridges; R: location on or close to a basement ridge.

Profile	Station	Water depth (km)	Crust Thick. (km)	*Vp* Layer 2 (km s^{-1})	*Vp* Layer 3 (km s^{-1})	*Pn* Refract. (km s^{-1})	Position	Class
Western Volcanic Zone								
20010170	171	3.8	3.2	2.4–3.6	–	7.6		1
	172	3.8	1.2	3.2–4.3	–	7.6		1
20010180	181	3.8	4.9	2.4–5.2	–	7.6		2
20010190	191	4.0	2.5	3.0–5.0	–	7.7		2
Sparsely Magmatic Zone								
20010150	151	4.9	2.5	3.5–5.4	–	7.4	NTS	2
	152	–	–	–	–	–	–	–
20010160	161	4.0	1.4	4.0–6.0	–	7.7	NTS/R	3
20010200	201	4.7	1.9	3.4–4.9	–	7.8	R	2
20010210	211	4.5	2.1	3.9–6.2	–	7.7	NTS	3
Eastern Volcanic Zone								
20010220	221-west	4.0	2.7	3.0–6.4	–	7.6	NTS/R	2
	221-east	4.0	2.7	4.2–6.1	–	7.6	NTS	3
	222	4.5	2.6	3.9–5.4	–	7.6	NTS	2
20010230	231	4.3	2.7	3.0–4.2	–	7.5	NTS	1
	232	4.0	3.3	3.2–6.1	–	7.7	R	2
20010240	241	4.5	2.9	3.6–4.9	–	7.7	NTS	1
	242	–	–	–	–	–	–	–
20010250	251	4.8	3.5	3.2–6.0	–	7.7	R	2
Knipovich	**Ridge**[a]	3.2	3.7	4.0–4.5	–	8.0		
Knipovich	**Ridge**[b]	3.4	5.5	3.5–7.1	–	7.6		
Mohns	**Ridge**[c]	3.2	4.0	2.5–3.0	5.8–6.8	7.2–7.6		
SW Indian	**Ridge**[d]	3.0–4.2	3.0–6.0	3.0–6.4	6.5–7.0	8.0		
Molloy	**Ridge**[e]	2.0	4.0	**	6.6–7.1	7.9		

[a]Ritzmann *et al.* (2004),[b]Ljones *et al.* (2004),[c]Klingelhöfer *et al.* (2000),[d]Muller *et al.* (1999),[e]Czuba *et al.* (2005) (**no upper crustal velocities were modelled).

of the crust. The Pn phase can be correlated with some confidence up to an offset of 20 km and has a velocity of 7.7 km s^{-1}. According to our model, the crustal thickness varies between 1.4 and 1.5 km. Based on the velocity information, it is evident that oceanic layer 3 is completely absent or is so thin that it cannot be resolved by our experimental set up. It could be that along this profile the crust is absent and the seafloor consists only of altered mantle rocks.

Line 20010210 (Figs 8 and 10b)

At station 211, a clear phase from the oceanic crust is observed for a larger distance. The crustal phase is almost 4 km long and has a velocity of 4.0 km s^{-1}. No velocities higher than 5 km s^{-1} can be identified in the section, but have been modelled to some extent to fit the observed and modelled traveltime curves. A phase with a velocity of 7.7 km s^{-1} occurs at approximately 10 km offset. The small traveltime undulations of this phase mainly follow the bathymetry. The transition from crust to mantle seems to happen in a narrow zone with a high velocity gradient. Crustal velocities of 3.9 km s^{-1} at the seafloor and 6.2 km s^{-1} at the bottom of the crust have been modelled. The crustal thickness is 2.1 km.

The Eastern Volcanic Zone (29°E–85°E)

In general, this zone is shallower than the SMZ and has large axial volcanoes east of 55°E. Four magmatic basement ridges cross the rift valley at right angle to its strike direction (Fig. 1, C–F). This segment is best investigated by recording stations and shows the best data quality. It also exhibits a major change in strike of the Gakkel Ridge, at 60°E. The easternmost station is located close to this area. East of basement ridge F (Fig. 1), seismic reflection data show that the rift valley is almost completely covered by sediments (Kristoffersen 2001; Jokat & Micksch 2004).

Line 20010230 (Figs 9 and 10c)

This model is constrained by two recording stations separated by 50 km. The water depths at the endpoints of this profile are 4.3 km (station 231) and 4.0 km (station 232), and drop down to 5.0 km in the middle of the profile. For station 232 (Fig. 10c), the two-layer model starts with a velocity of 3.2 km s^{-1} at the seafloor, and reaches 4.9–5.3 km s^{-1} at the base of the first layer. Lower crustal velocities range between 5.8 and 6.1 km s^{-1}. Only one layer was modelled beneath station 231 (Fig. 9), with seismic velocities from 3.0 to 4.2 km s^{-1} to fit the traveltime curve. The crustal thickness is also constrained by a PmP phase at 9–13 km offset. The mantle refraction has almost the same intercept time in both sections, and its seismic velocity ranges between 7.5 and 7.7 km s^{-1}. The crustal thickness varies between 2.7 km (231) and 3.3 km (232) (Fig. 10c). Eastward thickening of the crust is also documented by the Pg phase at station 232, which can be observed over larger offsets.

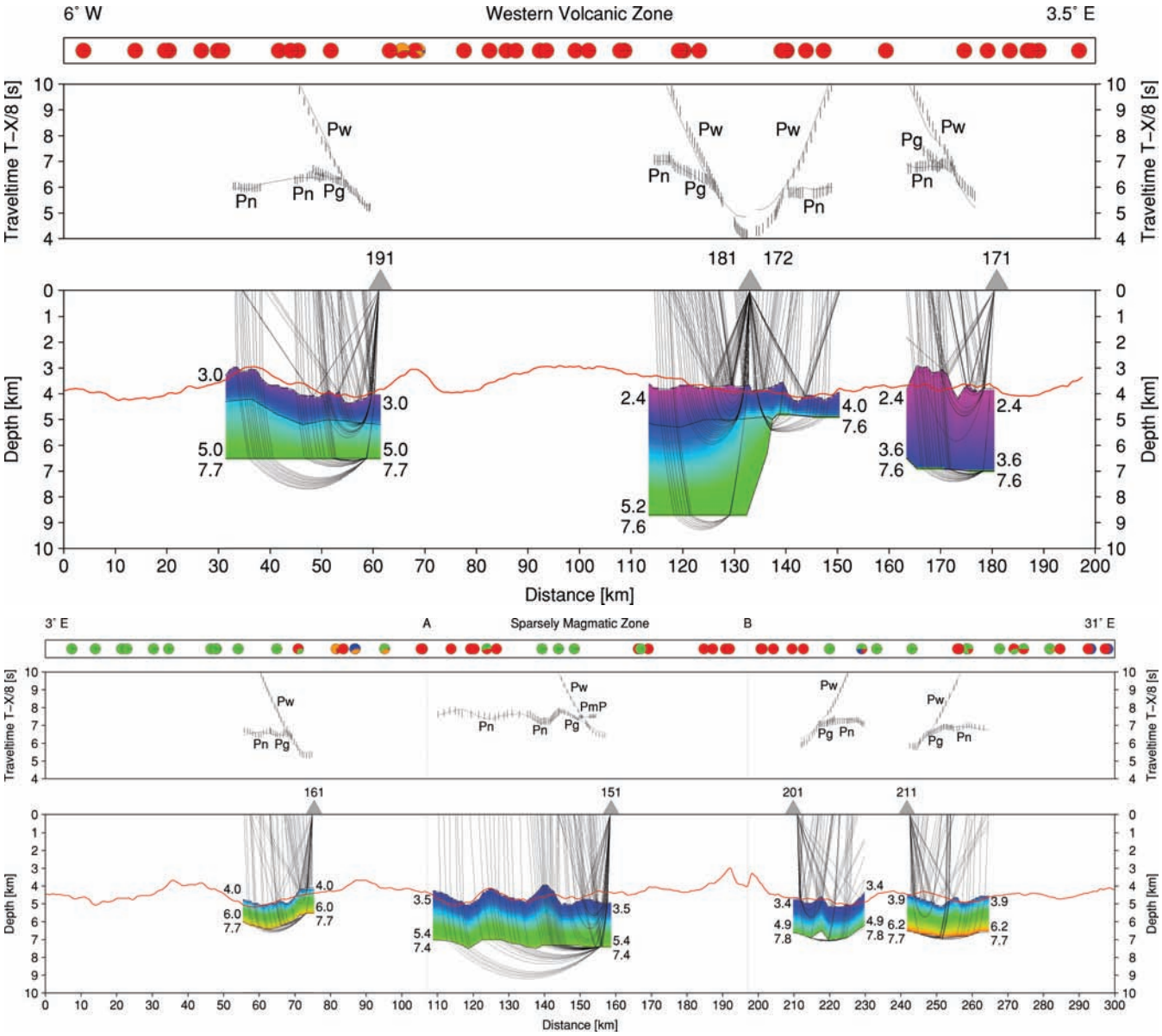

Figure 10. Summary of the modelled seismic stations along the rift valley. Top panel: Picks (vertical bars), modelled traveltimes for all stations of (a) the WMZ, (b) the SMZ, and for (c) the EVZ are shown. Bottom panel: Depth models of *P*-wave velocities and ray coverage for all stations of (a) the WMZ, (b) the SMZ, and for (c) the EVZ are shown. Note that stations 171 and 172 have a poor data quality compared to the other record sections (see Fig. 11). However, the significantly different intercept times for the mantle phase indicate that the crustal fabric in the area around 3°30′E might change quite rapidly. Thus, interpretations of the two stations should be made with care. The basement ridges A–F are marked to show correlations between their locations and variations in crustal thickness. Triangles mark the location of the seismic recording stations. Note that on top the results of the dredges are plotted as circles (red: Basalt; green: Peridotite, orange: Gabbro, blue: others) displaying the percentage of each rock type in the dredge, respectively. Solid red lines in the bottom panel mark the bathymetry along the rift valley.

DISCUSSION

The best areas to test some of the hypotheses for seafloor spreading processes are the end-members of the global ridge system. Such ridges are important to test whether the predictions of general models apply at their extremes. One candidate for the slow spreading rate end is the Gakkel Ridge. The striking characteristic, besides the ultraslow spreading of this ridge, is the almost complete absence of fracture zones, whose existence might otherwise bias interpretation of the petrological and geophysical data. We first discuss the results from the three segments before drawing some general conclusions.

The Western Magmatic Zone

In the WMZ, the ridge has a completely different bathymetric and magnetic character than along the rest of the Gakkel Ridge. Five elongated rift-parallel volcanic ridges were mapped in a 220 km long segment. The ridges rise some 0.4–1.3 km above the axial valley floor at 4.2 km, and are 15–50 km long (Michael *et al.* 2003). One even more pronounced difference of this segment, in comparison to the rest of the ridge, is observed in its magnetic field. While the axial magnetic anomaly varies in the SMZ from almost 0 to 500 nT, the WMZ magnetic anomaly shows large amplitudes of up to 1000 nT

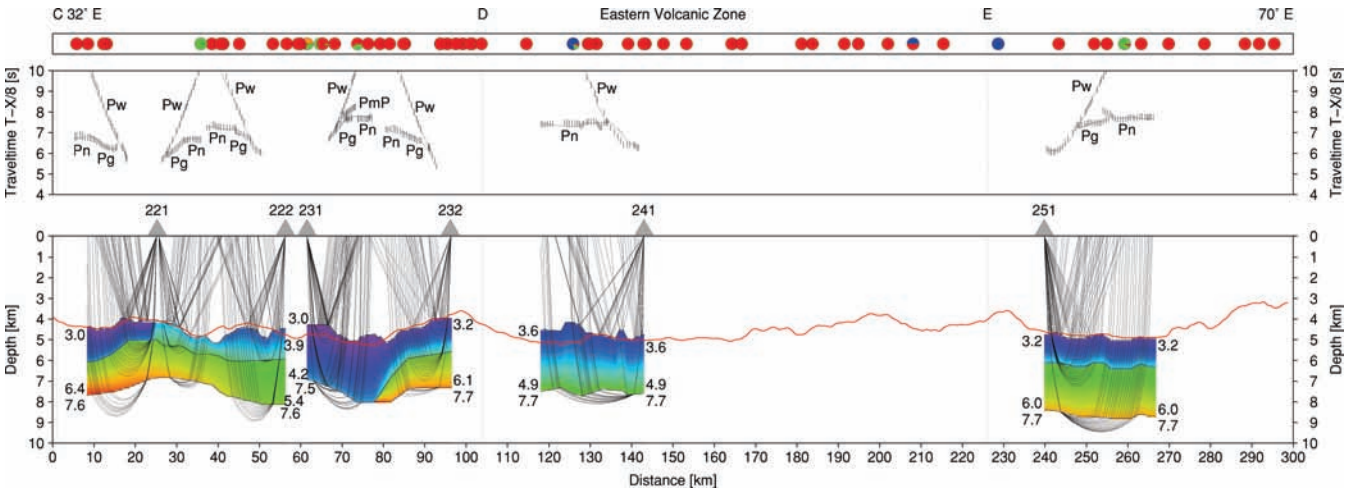

Figure 10. (*Continued.*)

between the northern Lena Trough and the eastern termination of the segment at 3°30′E. Here, the new magnetic data indicate that the axial anomaly decreases from peak values of 300 to 10 nT over a distance of 29 km. For almost 80 km east of this boundary only peridotites were dredged, as opposed to predominantly basalts west of 3°30′E. Seismic station 181, towards the west, shows again greater values (4.9 km) for the crustal thickness. Together with the bathymetry (Michael *et al.* 2003), the data can be interpreted in such a way that the western branch of station 181 maps the deeper structure of one of the elongated volcanic ridges, which are underlain by thicker oceanic crust. In addition to the variations in crustal thicknesses, the velocity–depth models also vary. Velocities above 6.5 km s^{-1}, which are typical for oceanic layer 3, are not visible in any section.

The crustal thickness at station 181 is close to the crustal thickness of 6–7 km reported by Kristoffersen *et al.* (1982) at 7°W (∼100 km west of station 181). However, below station 191, some 50 km west, the crustal thickness decreases again to 2.5 km. The data show (Table 1), that in this segment, the crustal thickness is still highly variable, but that this variability is not reflected in variations in the magnetic field. No basement ridges are present like those in the other two segments. A more detailed interpretation is difficult due to the absence of a more comprehensive seismic data set in this segment.

The western part of the Gakkel ridge (west of 3°30′E) might be fed by a different mantle source. It formed almost 20 Myr later than the eastern branch, when the Morris Jessup Rise and Yermak Plateau formed and separated at around 35 Ma (Vogt *et al.* 1979; Michael *et al.* 2003). Possibly, enhanced melt production resulted in slightly faster spreading and topographic features that are completely different to those in the east. The higher melt production is also manifested in the continuous and strong magnetic anomaly along the rift valley of the Gakkel Ridge.

The Sparsely Magmatic Zone

The rift valley of the Gakkel Ridge is deepest in the SMZ (3°E–29°E). The SMZ is likely to be the most extreme expression of an ultraslow spreading ridge. In the west, at 3°30′E, there is a sharp boundary in both the petrological composition of the rocks and magnetic data. Within 20 km, the central anomaly drops from almost 500 nT to zero (Fig. 3). In conjunction with this, the rift valley deepens by almost 1.1 km, and there is a non-transform offset (Michael *et al.* 2003). Predominantly peridotites were dredged in the SMZ and, consistent with this, the seismic models revealed the most extreme velocity–depth functions. There is little control on upper crustal velocity with traveltime branches visible in the data from only two stations (Fig. 10b; 151 and 211). The highest modelled *P*-wave crustal velocities are 5.4 to 6.2 km s^{-1}. The Pn arrival appears after very short distances (10 km), indicating thin oceanic crust. No clear PmP is visible on the seismic record sections, with the exception of station 151. However, FD modelling shows that PmP reflections would be visible only to a maximum offset of 10 km, at which range they are not masked by the strong arrivals of the water wave train. It is important to note that all stations in the SMZ have high amplitude arrivals between 6 and 10 km in common. This would not be the case if we were to consider layer 2 as a gradient zone, in which case a continuous decrease in seismic amplitudes would be expected. Such amplitude anomalies are common in the record section, when for example the reflected and refracted phases of the same layer boundary meet or have almost the same traveltime. Destructive and constructive interference of the two phases may create these high amplitude wave trains. The observed strong amplitudes originate, in our opinion, from constructive interference of the PmP and Pn arrivals. Thus, we consider this an indirect indication for the presence of a PmP phase. The thinnest crust in this segment was measured beneath station 161 (1.4 km) close to basement ridge A. This station is located in the long amagmatic segment of the SMZ. Station 151, immediately to the east, shows slightly higher crustal thickness (2.5 km), but a 0.9 km greater water depth and a very low Pn velocity of 7.4 km s^{-1}. From the seismic data, it is not clear if the seismic experiment sampled oceanic crust or altered mantle material, since almost no basalts were sampled in this part of the rift valley.

The Eastern Volcanic Zone

In the EVZ (29°E–85°E), the rift valley of the Gakkel Ridge east of 50°E shows again a different bathymetric characteristic. Just before and east of the only significant bend in the rift valley, at 60°E, large axial volcanoes start to dominate the bathymetry. The largest volcano occurs at 70°E. Further to the east, at 85°E, a smaller volcanic feature can be seen. Here, fresh basalts were dredged (Michael *et al.* 2003), which support interpretations of earthquake and side scan sonar data that recent or ongoing volcanic activity is present in

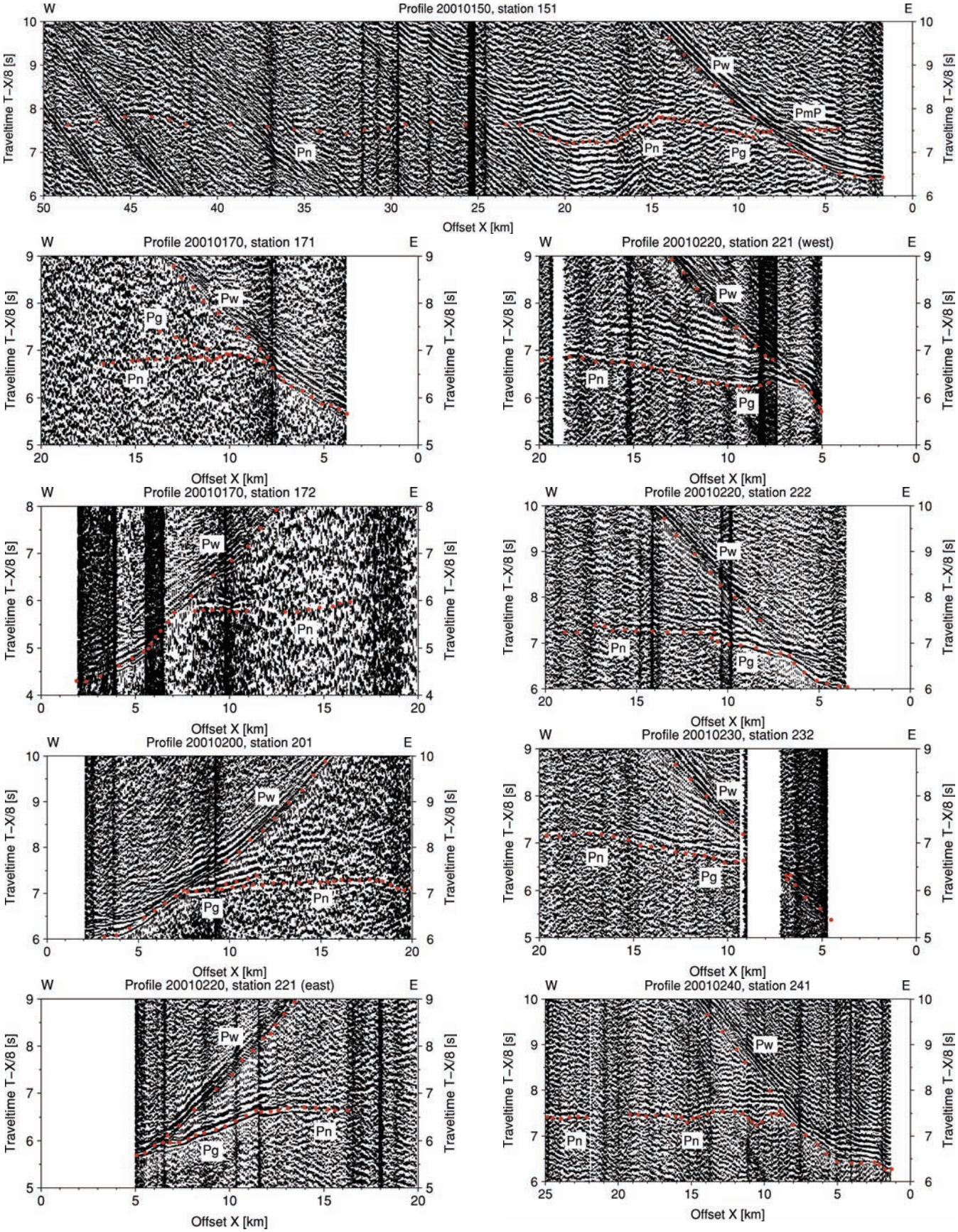

Figure 11. The remaining seismic sections.

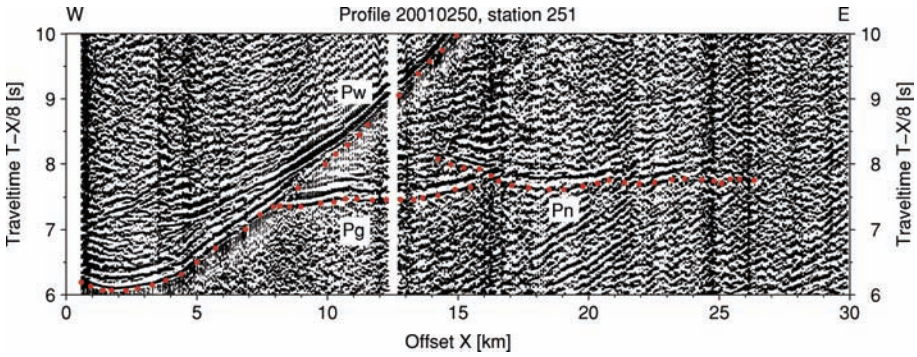

Figure 11. (*Continued.*)

this region (Müller & Jokat 2000; Edwards *et al.* 2001). Between the two volcanoes the rift valley topography is shallow and flat indicating that thick sediments cover the basement. Seismic reflection data across the rift valley east of 70°E, indicate sediment thicknesses of 1.0 km (Jokat & Micksch 2004). Thus, no direct information on the rift valley topography is available in the easternmost part of the Gakkel Ridge investigated during the AMORE expedition. The recording stations in the EVZ show a different characteristic for the upper basaltic layer than in the SMZ. Since clear arrivals of velocities well above 3.0 km s^{-1} and sometimes even 4.0 km s^{-1} are observed, the starting velocities for the uppermost layer have been chosen accordingly. Station 221, for example, is located on the eastern flank of basement ridge C and has two traveltime branches: one in the direction of the volcanic ridge, the other one towards a non-transform segment (Fig. 10c). The two models differ significantly in the thickness and velocity of the upper layer. Due to intercept times close to those of the seafloor reflections, the model for station 221-east starts with a velocity of 4.2 km s^{-1}, while its western branch shows only a velocity of 3.0 km s^{-1}. This is an indication that the basaltic cover in the area of the basement ridge C is thicker than in the non-transform segment. Basalts and peridotites were dredged beneath the eastern traveltime curve. Here, magmatic activity is not sufficient to carpet the valley completely with basaltic rocks. The high velocity of the upper layer does not prove the absence of basalts, as a low-velocity basalt unit that is not thick enough to have a significant effect on traveltimes may be present. This observation might indicate that mantle rocks, although altered, are close to the seafloor. It is also remarkable that the crustal thickness in the EVZ is not as thin as in the SMZ, although according to spreading models the half rates decrease towards the Laptev Sea. In the east, thicknesses do not drop below 2.5 km. A simple correlation between the results of the two segments is not possible. At first, basement ridges are bathymetrically not as pronounced in the SMZ as they are in the EVZ. Furthermore, more stations are located close to the basement ridges C-E than in the SMZ. The increased magmatism along these structures has created a different crustal structure. The easternmost station 251 is in an area near a large volcanic construction, and a strong bend of the rift valley. In the SMZ, mainly the basins in between ridges were sampled. Nonetheless, this supports the argument (Jokat *et al.* 2003) that no clear correlation between spreading rate and crustal thickness exists at ultraslow spreading rates. Data in the ridge segment east of 80°E are needed to quantify the crustal thickness at the lowest spreading rates.

Modelling of seismic data shows that the crustal velocity distribution along the Gakkel Ridge changes from station to station. Crustal velocities above 6 km s^{-1} are found at locations where volcanic constructs dominate the rift valley indicating that more magmatic material intruded the crust. In the EVZ and SMZ, these constructs are either basement volcanic ridge or axial volcanoes. These lower crustal velocities (>6 km s^{-1}) disappear away from the volcanic constructs. In between these features, the oceanic crust might only consist of a thin veneer of basalts directly underlain by mantle material, or the basalts may be absent. Layer 3, which in normal oceanic crust comprises gabbroic material, is absent.

Despite the variability of the velocity depth functions along the Gakkel Ridge, the different record sections can, in general, be divided into three classes (Table 1, Figs 10a–c):

Class 1: The first one shows slow second arrivals (<4 km s^{-1}), which provide evidence for an altered basaltic cover. Most of these stations (171, 172, 231 and 241) are modelled with a very simple velocity gradient in the absence of any other information. All are located in the segments between the basement ridges. Velocity–depth functions, however, vary from location to location, consistent with a variable basalt cover. Here, the crustal thickness varies between 1.2 and 3.2 km.

Class 2: The second class of record sections has some intermediate velocity depth functions. Velocities below and above 4 km s^{-1} are present in the traveltime curves. These stations (151, 201, 221-west, 222, 232 and 251) are either located on basement ridges or their flanks. The stations recorded evidence for both the basaltic cover and the thicker oceanic lower crust due to increased magmatism in those zones. Crustal thicknesses beneath these stations vary from 1.9 to 3.5 km. Stations 181 and 191 fall into this class, but instead of imaging a basement ridge, they provide information on large axial volcanoes in the WMZ—oceanic crust beneath a magmatically highly active structure. These stations show crustal thicknesses of 2.5–4.9 km.

Class 3: The third class of seismic records (stations 161, 211, 221-east) is marked by high *P*-wave velocities directly at the seafloor. The first velocities for the uppermost layer are close to or above 4 km s^{-1}. The intercept times of the fast traveltime branches are so close to those of the seafloor reflection that either no basalts are present or they are so thin that they cannot be detected by our experimental setup. These stations lie also in areas where mainly peridotites were sampled. Here, it is very likely that no crust exists and the mantle crops out at the seafloor as the sampling suggests. In this case, the modelled crust–mantle boundary is not the base of the crust, but indicates the lowermost boundary of altered peridotites.

Magnetic anomalies and the presence of peridotites

A correlation is observed between the strength of the magnetic rift valley anomaly and the occurrence of peridotites in the SMZ and

EVZ (Fig. 3). At at least three locations at 3°30′E, and the basement ridges B and C, this correlation is excellent. Where the magnetic anomaly reaches its minimum relative to at these volcanic centres, peridotites are dredged instead of basalts. For the rest of the basement ridges, the data coverage is not sufficient to claim such a correlation. In our research area, magnetic signals disappear completely in areas where peridotites predominate. A comparison of the velocity of the upper layer between the segments shows that the velocities are lowest in the WVZ and significantly higher in the EVZ and SMZ. If we relate the strength of the magnetic anomalies to the thickness of extrusive basalts in the rift valley, then magmatic activity in the WMZ should be significantly higher. We interpret these observations as indicating that a thin veneer of basalts produces the magnetic anomaly along the rift valley. This strongly supports models that suggest it is a thin (up to 0.5 km thick) basaltic layer that causes the magnetic signature of seafloor spreading anomalies (Schouten *et al.* 1999). The alternative, that the magnetization is provided by rocks in layer 3 (Hosford *et al.* 2003) cannot be confirmed for the Gakkel Ridge, because seismic refraction data show that layer 3 arivals do not exist, there.

Comparison with other slow/ultraslow ridges

To compare the results from the Gakkel Ridge with those of other ridges it is important to consider the spreading rates. Reid & Jackson (1981) proposed that the crustal thickness decreases sharply from the global mean of 7 km for oceanic crust (White *et al.* 1992) where full spreading rates fall below 20 mm yr^{-1}. If this model holds, mid-ocean ridges with rates in this range should all have similar crustal compositions. In the WVZ, the Gakkel Ridge has a maximum full spreading rate of 13 mm yr^{-1}, similar to the Mohns Ridge (16 mm yr^{-1}), the Knipovich Ridge (16 mm yr^{-1}) and the Southwest Indian Ridge (12–18 mm yr^{-1} at 66°E). Reported crustal thicknesses vary between 3 and 4 km (s. Table 1) for the investigated ridge segments. Low seismic velocities of up to 6.3 km s^{-1}, and the almost complete absence of velocities above 6.6 km s^{-1}, which are typical for oceanic layer 3, characterize the crust. At the Mohns Ridge, the crustal thickness varies along with the absence or presence of oceanic layer 3 (Klingelhöfer *et al.* 2000).

The Southwest Indian Ridge at 66°E exhibits crustal thicknesses of 3.5–6.0 km beneath the segment midpoints and 2.0–2.5 km in the non-transform segments. Along all profiles with such thin oceanic crust, very few or no arrivals are recorded from the uppermost layer. Thus, a velocity depth function is assumed to fit the onset of the later phases (Muller *et al.* 1999; Klingelhöfer *et al.* 2000). The latter authors modelled the extrusive parts of the Southwest Indian Ridge crust with a uniform thickness of 1.2 km (layer 2 *P*-wave velocity 3.0–6.4 km s^{-1}) and a highly variable thickness for layer 3 (*P*-wave velocity 6.5–7.0 km s^{-1}). Comparing Gakkel Ridge volcanic ridges with the Southwest Indian Ridge structure in those parts where spreading rates are closest to those at the Gakkel Ridge, it is striking that Sauter *et al.* (2004) also found features that seem to be loci of focused magmatism. Along the Southwest Indian Ridge, these features are located in the centres of spreading segment, and are separated by transform faults. The transform faults might develop where differences in accretion style between two foci are greatest, and thus represent the weakest part of a segment. Since the general shape of the Gakkel Ridge mirrors the Barents Sea shelf as well as the margin of the Lomonosov Ridge, we suggest that the melt supply along the Gakkel Ridge was never sufficient to allow the development of transform faults with a significant offset.

Finally, seismic data confirm earlier results, in a global context, that spreading rates correlate with the thickness of oceanic crust. However, below a certain threshold, which might be around 14 mm yr^{-1} full-rate (Jokat *et al.* 2003) this is no longer true. The magmatic activity at ultraslow spreading rates does not produce a consistent pattern of features in the rift valley. Large axial volcanoes might dominate a region and create a thick crust comparable to that at slow spreading ridges. The more or less regular pattern of basement ridges A–F, as seen in the SMZ and western part of the EVZ, are most likely typical for ultraslow ridges. The crustal composition is thus influenced by magmatic centres (Fig. 1, ridges A–F) and not by spreading velocities in this part of the Gakkel Ridge (Jokat *et al.* 2003; Michael *et al.* 2003). Such magmatic centres also exist at other ultraslow ridges or ridges with spreading rates close to the 14 mm yr^{-1} threshold (Muller *et al.* 1999; Géli *et al.* 1994; Okino *et al.* 2002; Sauter *et al.* 2004). Although the spacing and shape of these ridges vary, they can be considered to be a typical element of ultraslow ridge topography. That these ridges are most pronounced along the Gakkel Ridge might support the interpretation that this ridge is the slow spreading end-member of the world's ridge system.

Slow spreading ridges also tend to be characterized by slow upper mantle velocities, which vary from 7.6 to 7.8 km s^{-1} along the ridges (Table 1). The most common explanations for the low velocities are higher temperatures or serpentinization of upper mantle rocks. In the WVZ, we favour the interpretation that most of the velocity effect is caused by a hotter mantle than in the more easterly segments. The strong magnetic anomaly along the WVZ and the dredged basalts indicate that the mantle below the rift valley allows a higher melt production to produce these characteristics compared to the eastern parts of the ridge. The amount of serpentinization of mantle rocks to explain the lower Pn velocities is difficult to assess for this study. We think that deep reaching faults are present at the ridge, which would favour the penetration of sea water to deeper crustal levels. If we assume that a mantle velocity of 7.8 km s^{-1} is normal for the mantle below ultraslow ridges (Muller *et al.* 1999), the effect of additional serpentinization would have to account account for a decrease of up to 0.2 km s^{-1}.

CONCLUSIONS

The new seismic and magnetic data provide a unique insight into the structure of the rift valley of the western Gakkel Ridge. Both geophysical data sets vary greatly along the rift valley and appear, at first sight, to sample random variations. Linking the variations of the magnetic fields to the occurrence of the magmatic basement ridges explains the high magnetic anomaly amplitudes across the ridges. The lower magnetic signals in the non-transform segments mirror, to some extent, the presence or absence of basalts. Combining dredging results with information from the magnetic data, this interpretation is straightforward for regions where peridotites dominate dredges. In the other parts of the ridge the seismic data indicate that basalts have variable thickness, which might also influence the strength of the magnetic rift valley anomaly.

The velocity–depth function confirms the general interpretation from the magnetic and bathymetric data. The crustal composition below the magmatic centres (basement ridges A–F) is significantly different than in the non-transform segments. Lower crustal velocities above 6 km s^{-1} indicate the existence of intrusions due to the higher magmatic activity. However, oceanic layer 3 is completely missing along the investigated part of the Gakkel Ridge. Consistent with this, only very few Gabbros were dredged on the flanks

of the ridge. The variations of seismic velocities in the uppermost layer are related to a non-uniform thickness – or even an absence – of basalts at the seafloor. This raises questions about the composition of the layers underneath. We propose that below at least three stations (161, 211 and 221-east) and most likely also station 151, no 'normal' oceanic crust exists. Here, upper mantle material is exposed at the seafloor. The lower velocities can be explained by alteration or weathering of the peridotites. At other stations, which are also modelled with very low seismic velocities, the crust may consist of altered basalts. At these localities, magmatic activity was high enough to produce a thicker basalt cover than that for example, in the SMZ.

The results in the WVZ are somewhat surprising. While the strong magnetic anomaly and the changed rift valley topography suggest a rather homogenous crustal fabric, the seismic results show the opposite. Crustal thickness varies by a factor of more than 100 per cent in the seismic record sections.

The question of whether oceanic crust exists along some segments is difficult to answer using the seismic data of this study. The resolution of the 'crustal' velocity structure is not sufficient. Only secondary arrivals provide some constraints, along with Pn refractions, on the velocity structure. For solving problems like this, the receiver has to be positioned on the seafloor, and the seismic source has to be towed close to the seafloor. With current techniques, this is impossible in the Arctic Ocean.

Finally, models predicting a decrease in crustal thickness with spreading velocities are generally reliable. For these models, however, the Gakkel Ridge is a singularity, where the assumption no longer applies. Although the spreading velocity decreases towards the east, the crustal thickness does not decrease with it, but is controlled by magmatic activity along the ridge.

ACKNOWLEDGMENTS

We thank the captains and crews of RV Polarstern and the USCGC Healy for their excellent support during the expedition. The finite difference software was kindly provided by T. Bohlen. The final processing of the magnetic data was done by M. Voss. Special thanks to G. Eagles for carefully checking the manuscript spelling. Constructive reviews from Frauke Klingelhöfer and an anonymous reviewer are acknowledged. The figures were created with GMT (Wessel & Smith 1998). The programme RAYINVR (Zelt & Smith 1992) was used for the raytracing. This analysis was funded by the Deutsche Forschungsgemeinschaft.

REFERENCES

Bohlen, T., 2002. Parallel 3-D viscoelastic finite difference seismic modelling, *Computers and Geosciences*, **28,** 887–899.

Bown, J.W. & White, R.S., 1994. Variation of spreading rate of oceanic crustal thickness and geochemistry, *Earth planet. Sci. Lett.*, **121,** 435–449.

Coakley, B.J. & Cochran, J.R., 1998. Gravity evidence of very thin crust at the Gakkel Ridge (Arctic Ocean), *Earth planet. Sci Lett.*, **162,** 81–95.

Cochran, J.R., Kurras, G.J., Edwards, M.H. & Coakley, B.J., 2003. The Gakkel Ridge: Bathymetry, gravity anomalies, and crustal accretion at extremely slow spreading rates, *J. geophys. Res.*, **108**(B2), 2116, doi:10.1029/2002JB001830.

Crane, K., Doss, H., Vogt, P., Sundvor, E., Cherkashov, G., Poroshima, I. & Joseph, D., 2001. The role of the Spitsbergen shear zone in determining morphology, segmentation and evolution of the Knipovich Ridge, *Mar. Geophys. Res.*, **22,** 153–205.

Czuba, W., Ritzmann, O., Nishimura, Y., Grad, M., Mjelde, R., Guterch, A. & Jokat, W., 2005. Crustal structure of northern Spitsbergen along the deep seismic transect between the Molloy Deep and Nordaustlandet, *Geophys. J. Int.*, **161,** 347–364.

DeMets, C., Gordon, R.G., Argus, D.F. & Stein, S., 1994. Effect of recent revisions to the geomagnetic reversal time scale on estimates of current plate motions, *Geophys. Res. Lett.*, **21,** 2191–2194.

Dick, H.J.B., Lin, J. & Schouten H., 2003. An ultraslow-spreading class of ocean ridge, *Nature*, **426,** 405–411.

Duckworth, G.L., Baggeroer, A.B. & Jackson, H.R., 1982. Crustal structure measurements near FRAM II in the Pole Abyssal Plain, *Tectonophysics*, **89,** 173–215.

Edmonds, H.N. *et al.*, 2003. Discovery of abundant hydrothermal venting on ultraslow-spreading Gakkel Ridge in the Arctic Ocean, *Nature*, **421,** 252–256.

Edwards, M.H., Kurras, G.J., Tolstoy, M., Bohnenstiehl, D.R., Coackley, B.J. & Cochran, J.R., 2001. Evidence of recent volcanic activity on the ultraslow-spreading Gakkel ridge, *Nature*, **409,** 808–812.

Géli, L., Renard, V. & Rommevaux, C., 1994. Ocean crust formation processes at very slow spreading centers: a model for the Mohns Ridge, near 72°N, based on magnetic, gravity, and seismic data, *J. geophys. Res.*, **99**(B2), 2995–3013.

Grevemeyer, I. & Weigel, W., 1996. Seismic velocities of the uppermost igneous crust versus age, *Geophys. J. Int.*, **124,** 631–635.

Hosford, A., Tivey, M., Matsumoto, T., Dick, H., Schouten, H. & Kinoshita, H., 2003. Crustal magnetization and accretion at the Southwest Indian Ridge near the Atlantis II fracture zone, 0–25 Ma, *J. geophys. Res.*, **108**(B3), 2169, doi:10.1029/2001JB000604.

Jackson, H.R., Reid, I. & Falconer R.K.H., 1982. Crustal structure near the Arctic Mid-Ocean Ridge, *J. geophys. Res.*, **87**(B3), 1773–1783.

Jakobsson, M. and IBCAO Editorial Board Members, 2001. Improvement to the International Bathymetric Chart of the Arctic Ocean (IBCAO): Updating the Data Base and the Grid Model, *EOS, Trans. Am. geophys. Un.*, **82**(47), Fall Meet. Suppl., Abstract OS11B-0371.

Jokat, W. & Micksch, U., 2004. The sedimentary structure of Nansen and Amundsen basins, *Geophys. Res. Lett.*, **31,** L02603, doi:10.1029/2003GL018352.

Jokat, W., Buravtsev, V. & Miller, H., 1995. Marine seismic profiling in sea ice covered regions, *Polarforschung*, **64**(1), 9–17.

Jokat, W. *et al.*, 2002. Geophysical Investigations, in *Polarstern Arktis XVII/2 – Cruise Report: Amore 2001*, Vol. 421, pp. 165–210, ed. Thiede, J., Berichte zur Polarforschung.

Jokat, W., Ritzmann, O., Schmidt-Aursch, M.C., Drachev, S., Gauger, S. & Snow, J., 2003. Geophysical evidence for reduced melt production on the ultraslow Gakkel Ridge (Arctic Ocean), *Nature*, **423,** 962–965.

Karasik, A.M., 1968. Magnetic anomalies of the Gakkel Ridge and origin of the Eurasia Subbasin of the Arctic Ocean, *Geophys. Methods Prospect. Arctic*, **5,** 8–19.

Klingelhöfer, F., Geli, L., Matias, L., Steinsland, N. & Mohr, J., 2000. Crustal structure of a super-slow spreading centre: a seismic refraction study of Mohns Ridge, 72°N, *Geophys. J. Int.*, **141,** 509–526.

Kristoffersen, Y., Husebye, E.S., Bungum, H. & Gregersen, S., 1982. Seismic investigations of the Nansen Ridge during the FRAM I experiment, *Tectonophysics*, **82,** 57–68.

Kristoffersen, Y., 2001. The Eurasia Basin: an update from a decade of geoscientific research, *Polarforschung*, **68,** 11–18.

Ljones, F., Kuwano, A., Mjelde, R., Breivik, A., Shimamura, H., Murai, Y. & Nishimura, Y., 2004. Crustal transect from the North Atlantic Knipovich Ridge to the Svalbard Margin west of Hornsund, *Tectonophysics*, **378,** 17–41.

Michael, P.J. *et al.*, 2003. Magmatic and amagmatic seafloor generation at the ultraslow-spreading Gakkel Ridge, Arctic Ocean, *Nature*, **423,** 958–961.

Müller, C. & Jokat, W., 2000. Seismic evidence for Volcanic Activity at the Eastern Gakkel Ridge, *EOS, Trans. Am. geophys. Un.*, **81**(24), 265, 269.

Muller, M.R., Minshull, T.A. & White, R.S., 1999. Segmentation and melt supply at the Southwest Indian Ridge, *Geology*, **27**(10), 867–870.

Okino, K., Curewitz, D., Asada, M., Tamaki, K., Vogt, P. & Crane, K., 2002. Preliminary analysis of the Knipovich ridge segmentation: Influence of focused magmatism and ridge obliquity on an ultraslow spreading system, *Earth planet Sci. Lett.,* **202,** 275–288.

Reid, I. & Jackson, H.R., 1981. Oceanic spreading rate and crustal thickness, *Mar. Geophys. Res.,* **5,** 165–172.

Ritzmann, O., Jokat, W., Mjelde, R. & Shimamura, H., 2004. Crustal structure between the Knipovich Ridge and the Van Mijenfjorden (Svalbard), *Mar. Geophys. Res.,* **23,** 379–401.

Sauter, D., Mendel, V., Rommevau-Jestin, C., Parson, L.M., Fujimoto, H., Mevel, C., Cannat, M. & Tamaki, K., 2004. Focused magmatism versus amagmatic spreading along the ultraslow spreading Southwest Indian Ridge: Evidence from TOBI side scan sonar imagery, *Geochem., Geophys., Geosys.,* **5**(10), Q10K09, doi:10.1029/2004GC000738.

Schouten, H., Tivey, M.A., Fornari, D.J. & Cochran, J.R., 1999. Central anomaly magnetization high: Constraints on the volcanic construction and architecture of seismic layer 2A at a fast-spreading mid-ocean ridge, the EPR at 9°30′–50°N, *Earth planet. Sci. Lett.,* **169,** 37–50.

Verhoef, J., Roest, W.J., Macnab, R., Arkani-Hamed, J. & members of the Project Team, 1996. Magnetic Anomalies of the Arctic and North Atlantic Oceans and Adjacent Land Areas, Open File 3125b, Geological Survey of Canada, Dartmouth, NS, Canada.

Vogt, P.R., Taylor, P.T., Kovacs, L.C. & Johnson, G.L., 1979. Detailed aeromagnetic investigations of the Arctic Basin, *J. geophys. Res.,* **84**(B3), 1071–1089.

Weigelt, E. & Jokat, W., 2001. Peculiarities of roughness and crustal thickness of oceanic crust in the Eurasian Basin, Arctic Ocean, *Geophys. J. Int.,* **145,** 505–516.

Wessel, P. & Smith, W., 1998. New improved version of Generic Mapping Tools released, *EOS, Trans. Am. geophys. Un.,* **79**(47), 579.

White, R.S., McKenzie, D. & O'Nions, R.K., 1992. Oceanic Crustal Thickness From Seismic Measurements and Rare Earth Element Inversions, *J. geophys. Res.,* **97**(B13), 19 683–19 715.

Zelt, C.A. & Smith, R.B., 1992. Seismic traveltime inversion for 2-D crustal velocity structure, *Geophys. J. Int.,* **108,** 16–34.